RSC Advances

PAPER

View Article Online
View Journal | View Issue

Cite this: *RSC Adv.*, 2023, **13**, 11495

Light and pH dual-responsive spiropyran-based cellulose nanocrystals†

Xiu Ye,[ab] Anzhe Wang,[c] Dongyang Zhang,[d] Peng Zhou*[b] and Pengli Zhu*[a]

Received 13th March 2023
Accepted 5th April 2023

DOI: 10.1039/d3ra01637d

rsc.li/rsc-advances

Reversibly light and pH dual-responsive spiropyran-based cellulose nanocrystals (SP-CNCs) is synthesized by the attachment of carboxyl-containing spiropyran (SP-COOH) onto cellulose nanocrystals (CNCs). The resulting structure and properties of SP-CNCs are examined by Fourier transform infrared spectroscopy (FT-IR), elemental analysis, transmission electron microscopy (TEM), atomic force microscopy (AFM), dynamic laser light scattering (DSL), ζ-potential measurements and ultraviolet-visible (UV-Vis) light absorption spectroscopy. SP-CNCs exhibit excellent photochromic and photoswitching properties. Spiropyran moieties on SP-CNCs can be switched between open-ring merocyanine (MC) and closed ring spiropyran (SP) forms under UV/Vis irradiation, leading to color changes. Moreover, SP-CNCs display improved photoresponsiveness, photoreversibility, fatigue resistance, and stability in DMSO than in H_2O. We further investigate the pH-responsive behavior of SP-CNCs in H_2O. SP-CNCs aqueous solution display different colors at different pH values, which can be directly observed by naked eye, indicating that SP-CNCs can function as a visual pH sensor. These results suggest that light and pH dual-responsive SP-CNCs possess great potential for applications in reversible data storage, sensing, optical switching and light-controlled nanomaterials.

Introduction

Stimuli-responsive materials can alter their physical/chemical properties upon external stimuli, such as light, temperature, magnetic fields, and pH. They have received extensive attention in recent years due to their unique properties and various potential application in controlled release agents, adaptive shape memory materials, responsive coatings, *etc.*[1–8] Spiropyran, as one of the most classical stimuli-responsive materials, undergoes reversible structural isomerization upon a variety of stimuli, such as light, pH, temperature, metal ions, and solvent polarity.[9–12] Spiropyran-based materials have been extensively investigated and widely applied in many fields, such as bioimaging, controlled release, data storage, and sensors.[13–16]

There has been great interest in developing stimulus-responsive nanoparticles ascribing to their advantages such as, good water dispersibility, excellent biocompatibility and the ability for further functionalization.[17] Spiropyran has been used to functionalize various nanomaterials, such as gold or silver nanoparticles, semiconductor quantum dots, and carbon-based nanomaterials, to gain multifunctional materials to widen their field of applications.[18–20] Cong *et al.* have reported spiropyran-functionalized gold nanoclusters with controlled reversible dual-color fluorescence, which can be used for accurate fluorescence imaging.[18] Chen *et al.* have prepared spiropyran-functionalized carbon nanoparticles showing good photoreversibility upon UV/Vis irradiation. This has given rise to potential applications in bioimaging, reversible data storage/erasing, and light-controlled nanomaterials.[19] Moreover, Liao *et al.* have reported spiropyran-modified silicon quantum dots with good reversible photoluminescence that can be a promising candidate in many potential application areas such as biolabeling, bioimaging, photo-switch, and data storage.[20]

Cellulose nanocrystals (CNCs) are sustainable and renewable rod-shaped nanoparticles with high crystallinity, high aspect ratio and surface area, and which can be extracted from cellulose fibrils through strong acid hydrolysis processes.[21] Compared with the conventional nanoparticles, CNCs have been great interest to researchers due to their advanced properties, for instance, environmentally benign, naturally abundant, biocompatible, and biodegradable.[22] CNCs have been widely applied in various fields, such as nanocomposite materials, drug delivery, sensing, bioimaging and packaging.[23–28] CNCs have been reported to be used for sensing and responding to pH, metal ions, temperature, and humidity.[29,30] However,

[a]*Shenzhen Institutes of Advanced Electronic Materials, Shenzhen Institutes of Advanced Technology, Chinese Academy of Sciences, Shenzhen 518055, China. E-mail: yx444131997@gmail.com; pl.zhu@siat.ac.cn; Tel: +86-755-26731946*

[b]*Institute of Intelligent Manufacturing Technology, Shenzhen Polytechnic, Shenzhen 518055, China. E-mail: zhoupenghit@szpt.edu.cn*

[c]*School of Materials Science and Engineering, Nanjing Institute of Technology, Nanjing 211167, China*

[d]*Institute of Critical Materials for Integrated Circuits, Shenzhen Polytechnic, Shenzhen, 518055, China*

† Electronic supplementary information (ESI) available. See DOI: https://doi.org/10.1039/d3ra01637d

CNCs is still rarely reported as multi-stimulus responsive nanomaterials.

Spiropyran-based CNCs have not been reported to our knowledge. Herein, we successfully synthesized light and pH dual-responsive spiropyran-based cellulose nanocrystals (SP-CNCs) through the covalently linking between CNCs and carboxyl spiropyran (SP-COOH). SP-CNCs preserved the original properties of spiropyran, and exhibited excellent photochromic properties, photoresponsiveness, photoreversibility, fatigue resistance and stability. Moreover, SP-CNCs aqueous suspensions exhibited a pH-responsive behavior, different colors could be observed with the naked eye at different pH values. This novel dual-stimuli-responsive nanomaterial could be potentially used for various applications such as bioimaging, reversible data storage/erasing, sensing, and light-controlled nanomaterials.

Experimental section

Materials

CNCs were purchased from ScienceK Ltd (Shanghai China), which were extracted from microcrystalline cellulose through a sulfuric acid hydrolysis process. Epichlorohydrin, 5-nitrosalicylic acid, pyridine, *p*-dimethylaminopyridine (DMAP), EDC·HCL were supplied by the Sinopharm Chemical Reagent Co., Ltd (Shanghai, China). All the chemicals were analytical grade and used without any further purification.

Synthesis of SP-COOH

SP-COOH was synthesized according to the procedure described by Chen *et al.* (Scheme S1†).[31] First, 3-bromo-propionic acid (4.8 g, 31.4 mmol) and 2,3,3-trimethyl-3*H*-indole (2.5 g, 15.7 mmol) were dissolved in CH_3CN (30 mL). The mixture was refluxed for 12 h. The resulting solution was evaporated, and the residue was washed with ethyl ether (50 mL) for 3 times. Then, 1-(2-carboxyethyl)-2,3,3-trimethyl-3*H*-indolium bromide (2.55 g, 52%) was obtained by recrystallized with acetone/dichloromethane (5/1, v/v). Second, 1-(2-carboxyethyl)-2,3,3-trimethyl-3*H*-indolium bromide (2.1 g, 6.73 mmol), 5-nitrosalicylaldehyde (1.13 g, 6.73 mmol) and triethylamine (1.5 mL, 10.7 mmol) were dissolved in ethanol (30 mL), and refluxed under nitrogen for 6 h. The precipitate was filtered and washed with cool ethanol. Finally, SP-COOH was obtained as yellow powder (1.91 g, 75%).

The analytical data of SP-COOH: ^{1}H-NMR (400 MHz, DMSO-d_6): (TMS, ppm) 1.07 (s, 3H), 1.19 (s, 3H), 2.49 (m, 2H), 3.40 (m, 1H), 3.46 (m, 1H), 6.02 (d, J = 12.0 Hz, 1H), 6.66 (d, J = 8.0 Hz, 1H), 6.78 (t, J = 8.0 Hz, 1H), 6.86 (d, J = 12.0 Hz, 1H), 7.13 (t, J = 8.0 Hz, 1H), 7.18 (s, 1H), 7.22 (s, 1H), 8.01 (dd, J = 12.0 Hz, 1H), 8.22 (d, J = 4.0 Hz, 1H) (Fig. S1†). ESI-MS: m/z: calcd. for $C_{21}H_{20}O_5N_2$: 380.4; found: 379.2 [M–H$^+$] (Fig. S2†).

Preparation of CNC-NH_2

Amino-modified CNCs (CNC-NH_2) were prepared following our previous study (Scheme 1).[32] First, epoxy–CNC was prepared by reacting epichlorohydrin (0.8 g) with CNCs (100 mL, 1 wt%) under alkaline conditions (1 M aq. NaOH) at 60 °C for 3 h. Second, the epoxy ring was opened with excess ammonium hydroxide (6 mL) to introduce amino groups onto CNCs. The reaction was carried out at 60 °C for 2 h. Finally, the suspension was dialyzed against deionized water for 5 days, and concentrated to 1 wt% using a rotary evaporator.

Preparation of SP-CNCs

Freeze-dried CNC-NH_2 (0.5 g) powder was dispersed into DMSO (50 mL) under stirring and mild sonication for 30 min. Next, SP-COOH (0.5 g), EDC (0.5 g), and DMAP (0.1 g) were gradually added, and the mixture reacted at 30 °C for 48 h. After reaction, the product was precipitated and washed with acetone until no fluorescence emission was present. Then, SP-CNCs was dispersed into water, and dialyzed against deionized water for 5 days. Finally, SP-CNCs suspension were concentrated, sonicated, and preserved in the dark at 4–10 °C. Solid SP-CNCs powder was also obtained by lyophilization.

Characterizations

NMR spectra were recorded using an INOVA-600 spectrometer (Varian, Inc., Palo Alto, CA, USA; in DMSO-d_6 solutions). Fourier transform infrared (FT-IR) spectra were recorded on a Nicolet 5700 spectrometer (Nicolet Instrument Corp., Madison, WI, USA) and analyzed over the wavenumber range from 400 to 4000 cm^{-1}, with the KBr-disk method for sample preparation. Elemental analyses (CHON) were obtained on a Vario EL cube elemental analyzer (Elementar Analysensysteme GmbH, Hanau, Germany).

Transmission electron microscopy (TEM) images were obtained on a JEM-2100 microscope (JEOL Ltd, Tokyo, Japan) operating at the voltage of 200 kV. Atomic force microscopic (AFM) images were obtained in a dynamic force mode (Cypher S, Oxford Instrument plc, Abingdon, UK) using an AC240TS tip (tip radius < 10 nm, resonance frequency 300 kHz, and spring constant 42 N m^{-1}). Dynamic laser light scattering (DLS) and ζ-potential were measured using the Malvern Zetasizer Nano-ZS (ZEN3600, Malvern Instrument Ltd, Malvern, UK).

The UV-Vis absorption spectra of CNCs were measured with a UV-Vis spectrophotometer (UV-6100PCS, Shimadzu Corp, Tokyo, Japan).

Results and discussion

Structure and morphology of SP-CNCs

The successful covalent linkage of SP groups onto CNCs surface was confirmed by FT-IR analysis, and the SP content was determined by elemental analysis. FT-IR spectra of SP-COOH, CNCs, CNC-NH_2, and SP-CNC are shown in Fig. 1. For SP-COOH, the absorption peaks at 1715, 1651, 1567 and 1088 cm^{-1} were assigned to C=O, C=C, Ar–C and C–O–C group, respectively, which further confirmed that SP-COOH were successfully synthesized.[33] For nanocellulose, the absence of IR peaks at 3368 (O–H), 2904 (C–H), 1430 (CH_2), and 1060 (C–O) cm^{-1} were associated with the native cellulose.[34] Comparing the spectra of CNCs and SP-CNCs, the new

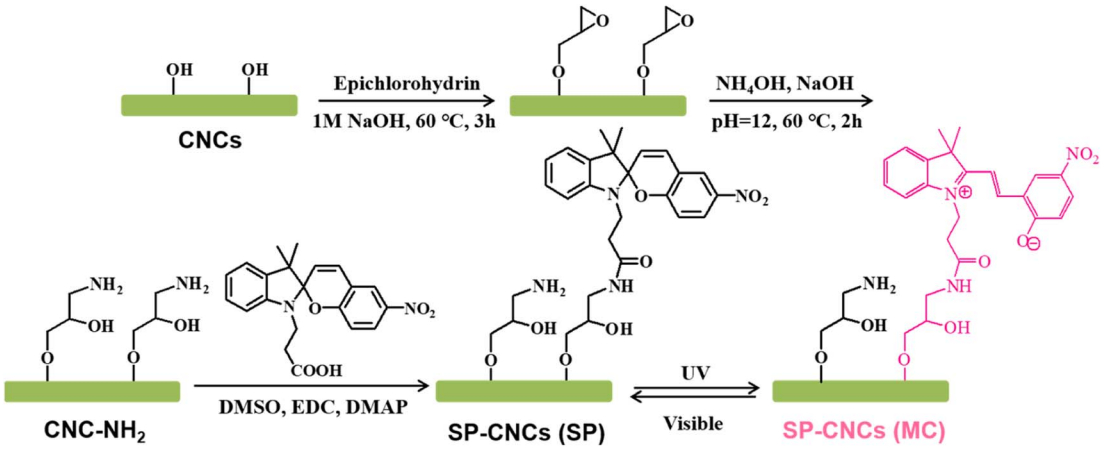

Scheme 1 Synthesis spiropyran modified cellulose nanocrystals (SP-CNCs), and photoisomerization of SP-CNCs (transition of spiropyran between SP and MC form upon UV/Vis light stimulus).

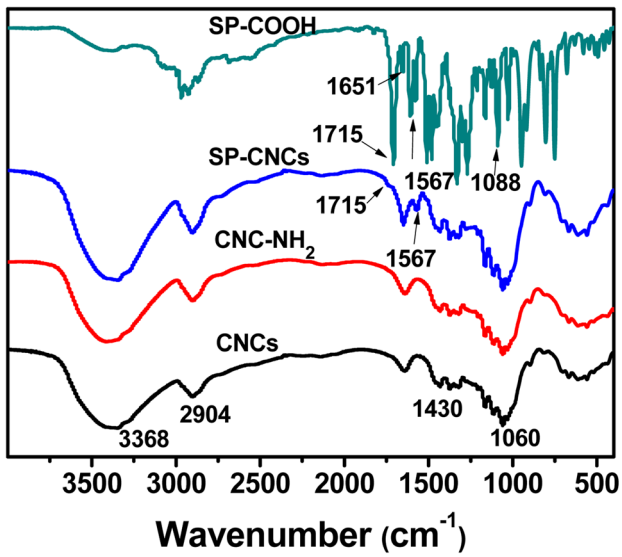

Fig. 1 FT-IR spectra of CNCs, CNC-NH_2, SP-CNCs and SP-COOH.

absorption peaks at 1715 and 1567 cm^{-1} were observed in SP-CNCs, which were assigned to C=O and Ar–C groups of SP-COOH, respectively. FT-IR results thus suggested that SP-COOH were successfully incorporated onto cellulose skeleton.

The elemental composition of CNCs, CNC-NH_2, and SP-CNCs are evaluated from elemental analysis (Table 1). CNCs contained no nitrogen (N) content, whereas the increased N content of SP-CNCs further confirmed the successful introduction of SP groups onto CNCs. The SP content on SP-CNCs was calculated from the N content of SP-CNCs using the following equation:

$$(1 \times 0.12\% + 2N \times m)/[1 + (380 - H_2O) \times m] = 0.23\%$$

where m is the molar number of SP reacted with 1 g of CNC-NH_2, and 380 is the molar mass of SP-COOH. The SP content (m) was calculated to be 40.49 μmol g^{-1} of CNCs (6.4 SP moiety per 1000 anhydroglucose units).

Table 1 Elemental analysis of CNCs, CNC-NH_2 and SP-CNCs

Sample	C (wt%)	O (wt%)	H (wt%)	N (wt%)
CNCs	41.49	—	6.51	0
CNC-NH_2	41.42	—	5.89	0.12
SP-CNCs	44.04	—	6.28	0.23

The morphologies of CNCs and SP-CNCs were investigated by TEM and AFM (Fig. 2). TEM images of CNCs and SP-CNCs are shown in Fig. 2a and b. The rod-like shapes of CNCs and SP-CNCs appeared not to have been changed, and SP-CNCs morphology did not alter after introducing SP groups onto CNCs surfaces. The length (L) and width (W) of CNCs and SP-CNCs were evaluated to be 50–350 nm and 5–30 nm, respectively.

From AFM images of CNCs and SP-CNCs, length (L) and width (W) information can be extracted (Fig. 2c and d). Length and width distribution histograms for CNCs and SP-CNCs were produced, with the mean values of length and width for CNCs were calculated to be 159 ± 70 nm and 20 ± 6 nm, respectively, and the mean aspect ratio (L/W) was 8.0 (Fig. 3). For SP-CNCs, the mean values of length and width were calculated to be 178 ± 64 nm and 21 ± 8 nm, respectively, with a mean aspect ratio (L/W) of 8.5. Due to the surface modification of CNCs with SP groups, the mean size of SP-CNCs was slightly larger than that of CNCs. In addition, the hydrodynamic radius (R_h) of CNCs and SP-CNCs dispersed in water were determined by DLS, with the mean R_h values for CNCs and SP-CNCs of 60.8 and 81.0 nm, respectively (Fig. 4). These results suggested that the apparent hydrodynamic radius of SP-CNCs increased slightly due to the introduction of SP groups onto CNCs. The surface charges of CNCs and SP-CNCs dispersed in water were estimated by ζ-potential measurement, with the ζ-potential values of CNC and SP-CNCs at −34.9 and −27.3 mV, respectively. After introduction of SP groups, the ζ-potential value of SP-CNCs was slightly increased due to the hydrophobic SP (closed-ring)

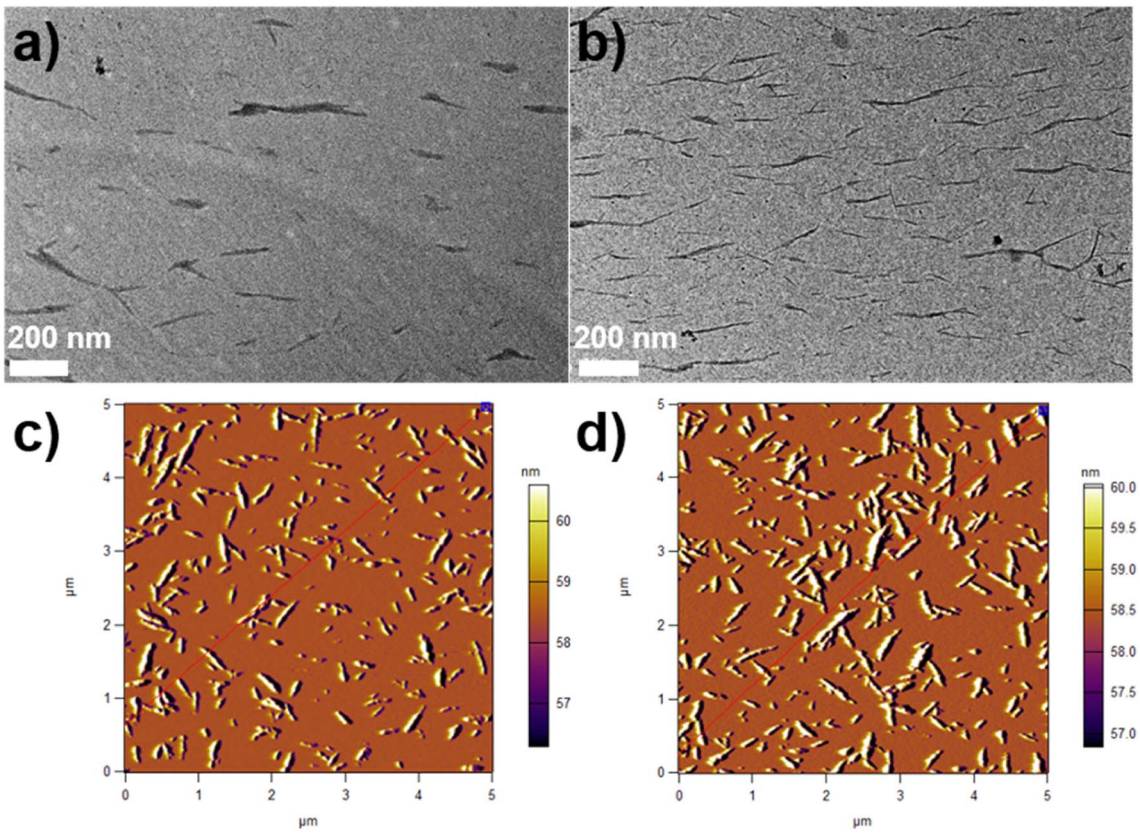

Fig. 2 TEM images of CNCs (a) and SP-CNCs (b, scale bar is 200 nm); AFM image of CNCs (c) and SP-CNCs (d).

isomerization. SP-CNCs were also well dispersed and stable in aqueous suspension, suggesting that the dispersibility was not significantly affected by surface modification of CNCs with SP.

Photochromic properties

It is well-known that the SP-based derivatives exhibit a reversible color change under UV (365 nm) and Vis irradiation.[9,35] To investigate the photochromic properties, SP-CNCs suspensions (0.5 wt%) in H_2O and DMSO were prepared and investigated by UV-Vis spectroscopy. Fig. 5a shows the absorbance spectra of SP-CNCs aqueous suspension upon exposure to UV irradiation from 0 to 6 min. There was no noticeable absorbance of SP-CNCs in range of 450–700 nm before UV irradiation, since most spiropyran structures on CNC were present as closed-ring forms (SP). Upon UV irradiation (365 nm), an apparent absorption peak at 525 nm was observed, which continuously and markedly increased with increasing irradiation time due to the transformation of SP into the open-ring (MC) isomers. Meanwhile, the color of SP-CNCs suspensions turned from colorless to pink, as the spiropyran structure gradually changed from SP to MC isomers. The zeta potentials of SP-CNCs were measured to be −21.0 mV (MC) and −13.7 mV (SP), indicating that the structure of spiropyran changed between the hydrophilic MC and hydrophobic SP isomers, which accordingly altered the distribution of charge in the molecule. When SP-CNCs were immediately irradiated with Vis light, the absorption peak at 525 nm rapidly decreased with increasing irradiation time. Following 90 s of Vis irradiation, the absorption peak was almost disappeared and completely restored to its value before UV irradiation. Meanwhile, the color of SP-CNCs turned from pink to colorless (Fig. 5b). These results suggested that SP-CNCs preserved the excellent photochromic properties of spiropyran.

Spiropyran-based polymers displayed different colors and photochromic properties due to of different extent MC isomers. Moreover, the MC isomers dissolved in different solvents exhibited different colors upon UV irradiation.[36] We further investigated the photochromic property of SP-CNCs in DMSO. Fig. 5c shows absorbance spectra of SP-CNCs aqueous suspension upon UV irradiation from 0 to 8 min. Before UV irradiation, no obvious absorbance of SP-CNCs was observed because most spiropyran structures on CNCs were present as closed forms of SP. Upon UV irradiation (365 nm), an apparent absorption peak at 560 nm was observed and continuously increased markedly with increasing irradiation time due to the transformation of SP into MC isomers. And the color of SP-CNCs suspension turned from colorless to purplish red. When SP-CNCs was immediately irradiated with Vis light, the absorption peak at 560 nm clearly decreased with increasing irradiation time, and almost disappeared after 120 s Vis irradiation. Meanwhile, the color of SP-CNCs turned from purplish red to colorless (Fig. 5d). The results demonstrate that SP-CNCs in DMSO also exhibited excellent photochromic properties.

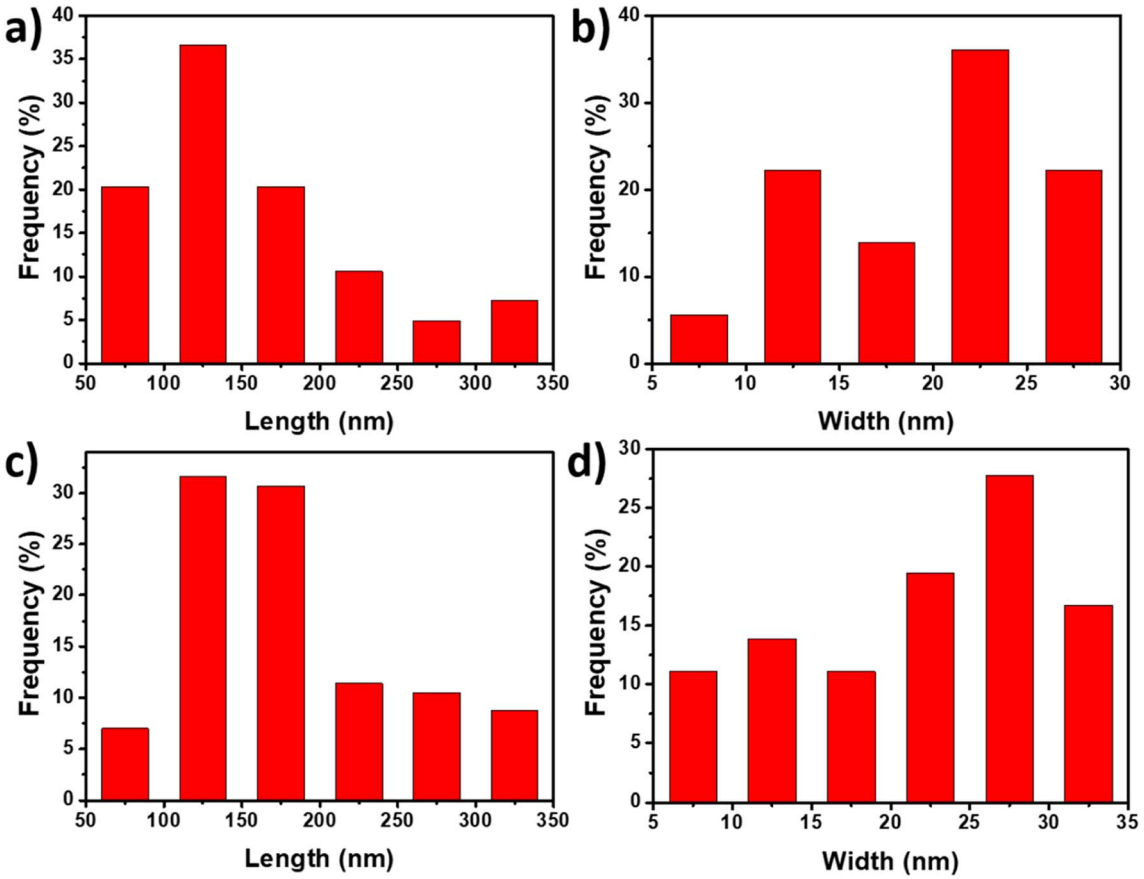

Fig. 3 Size distribution histograms of CNCs (a and b) and SP-CNCs (c and d) calculated from AFM images.

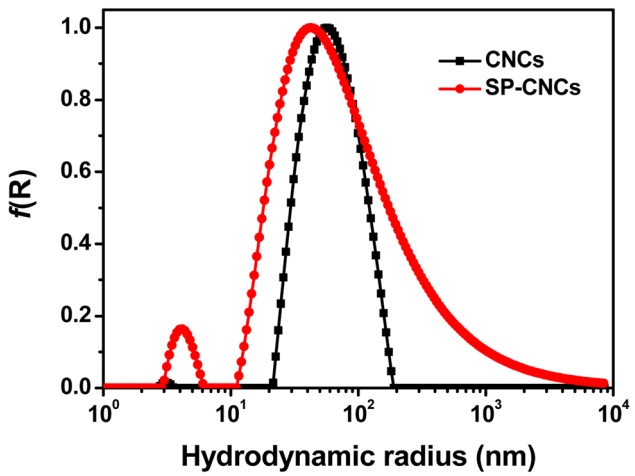

Fig. 4 Hydrodynamic radius (R_h) distributions of CNCs and SP-CNCs determined by DLS.

Photoreversibility and photofatigue-resistant properties were important indicators which can remarkably influence the final applications of photochromic materials.[37] To investigate photoreversibility and photofatigue-resistant properties, SP-CNCs suspension (0.5 wt%) in H_2O and DMSO were used to measure the absorbance intensity in maximum after UV (365 nm) and Vis irradiation for 10 cycles (Fig. 6). Furthermore, SP-CNCs in DMSO showed better fatigue resistance after 10 cycles of alternating UV/Vis irradiation than SP-CNCs in H_2O. Specifically, the maximum absorbance of SP-CNCs in DMSO was higher than that in H_2O, while the maximum absorbance of SP-CNCs in H_2O gradually decreased with 10 cycles of alternating UV/Vis irradiation. The fatigue behavior of SP-CNCs in H_2O was mainly caused by photodegradation. In addition, aggregated MC was difficult to immediately transform back to SP structures immediately and more likely to be affected by photodegradation.[38] These results suggested that their excellent photoreversibility and photofatigue-resistant properties could yield them applicable for practical used as anti-counterfeiting light-controlled, or sensing materials.

pH-sensitivity of SP-CNCs

We further studied the pH-responsive behaviors of SP-CNCs aqueous suspension at room temperature. SP-CNCs suspension at different pH values (2, 3, 4, 5, 6, 7, 8, 9, 10, 11, 12, 13) were prepared. As expected, SP-CNCs displayed rapid and distinct responses in the acid and alkali pH ranges. Fig. 7 shows the UV-Vis spectra of SP-CNCs aqueous suspension (0.5 wt%) at different pH values. It can be seen that SP-CNCs exhibited absorption peak changes at different pH values.

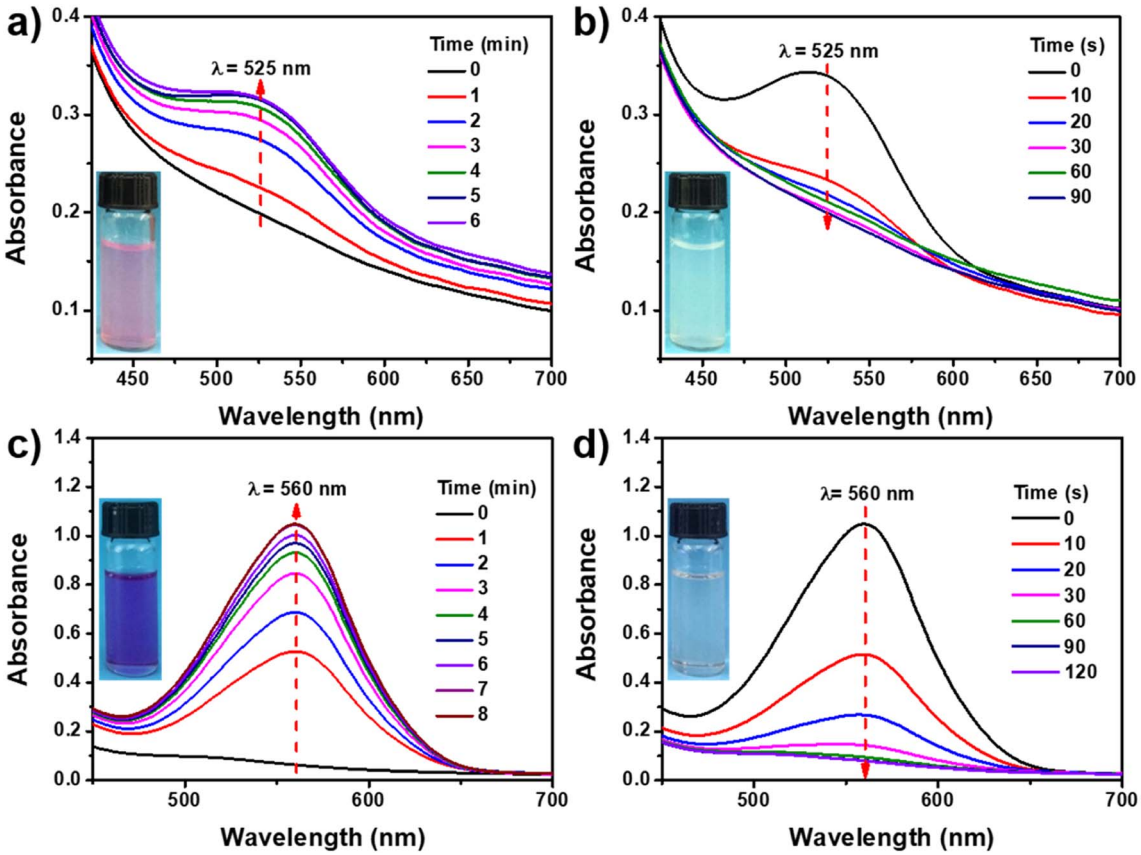

Fig. 5 UV-Vis absorption spectra of SP-CNCs (0.5 wt%) in H_2O (a and b) and DMSO (c and d) after irradiation with Vis and UV light (365 nm) for different times. Inset are the final photos of SP-CNCs suspensions after irradiation with UV (365 nm) and Vis light.

When the pH values were 2, 3, a strong absorption peak at 418 nm was observed. When the pH values were 4–10, there was a medium intensity absorption peak near 530 nm. When the pH values were 11–13, strong absorption peaks at 350 and 390 nm were observed. Therefore, the pH range of SP-CNCs aqueous suspension could be determined by UV-Vis absorption spectra measurement. Compared to the spectral method, colorimetric detection was more convenient. The results found that SP-CNCs aqueous suspensions at different pH values displayed different colors (Fig. 7). The color of the solutions at pH 2 and 3 (extreme acid) was light yellow, while the color of the solutions at pH 4–10 (weak acid, weak alkali and neutral) was pink. When pH values were 11–13 (extreme alkali), the color of the solutions was yellowish brown. These different

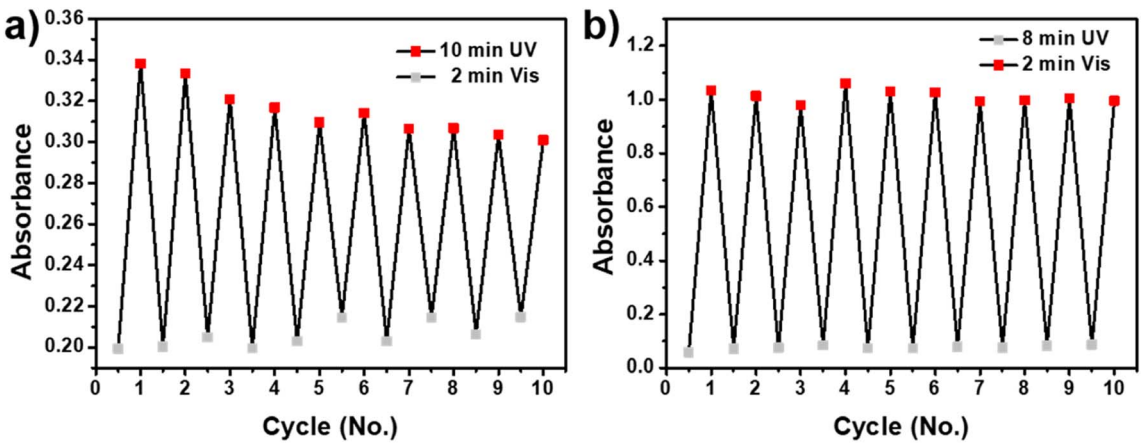

Fig. 6 Recyclability of the SP-CNCs (0.5 wt%) in H_2O (a) and DMSO (b). Changes in absorbance at 525 (H_2O, a) and 560 (DMSO, b) nm in the UV absorption spectrum of SP-CNCs solution under alternating irradiation with UV (10, 8 min) and Vis light (2 min) for 10 cycles.

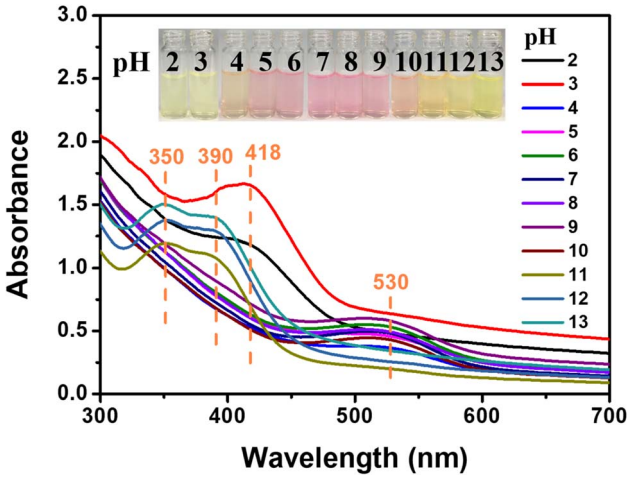

Fig. 7 UV-Vis absorption spectra of SP-CNCs aqueous solution (0.5 wt%) at different pH values (2, 3, 4, 5, 6, 7, 8, 9, 10, 11, 12 and 13). Inset denotes the photographic image of SP-CNCs aqueous solution at different pH values.

colors could be distinguished by the naked eye. The color changes in the pH response were mainly due to the presence or absence of H^+, which affected the different forms of spiropyran molecular ring opening, thus affecting the change of its UV absorption peak position.[39] Therefore, SP-CNCs aqueous suspension could be used as a colorimetric and spectral probe to determine pH in the range of 2–13.

Based on the above results and literature reports, we proposed a possible structural transformation process of photochromism and pH response based on SP-CNCs aqueous suspension (Fig. 8).[40,41] The SP form of SP-CNCs was transformed to MC form under UV irradiation, and MC form could be reversibly transformed to SP form under Vis irradiation. The MC form was protonated to MCH^+ form under acidic conditions and converted to SPH^+ form under strong acidic conditions. MCH^+ form could be converted into protonated SPH^+ form by Vis irradiation, which could be converted into SP form under alkaline conditions and MC form under strong alkaline conditions.

Conclusions

Novel reversibly light and pH dual-responsive spiropyran-based cellulose nanocrystals (SP-CNCs) were synthesized by grafting of carboxyl spiropyran (SP-COOH) onto CNCs surface. SP-CNCs displayed high stability, good photochromism properties, excellent photoreversibility and anti-fatigue properties. SP-CNCs aqueous solution also can be served as a visual pH sensor, which display different colors at different pH values. pH conditions could be directly determined through color changes, observed by naked eye. Thus, this dual-responsive nanomaterial may exhibit potential applications in bioimaging, reversible data storage, sensing and light-controlled nanomaterials.

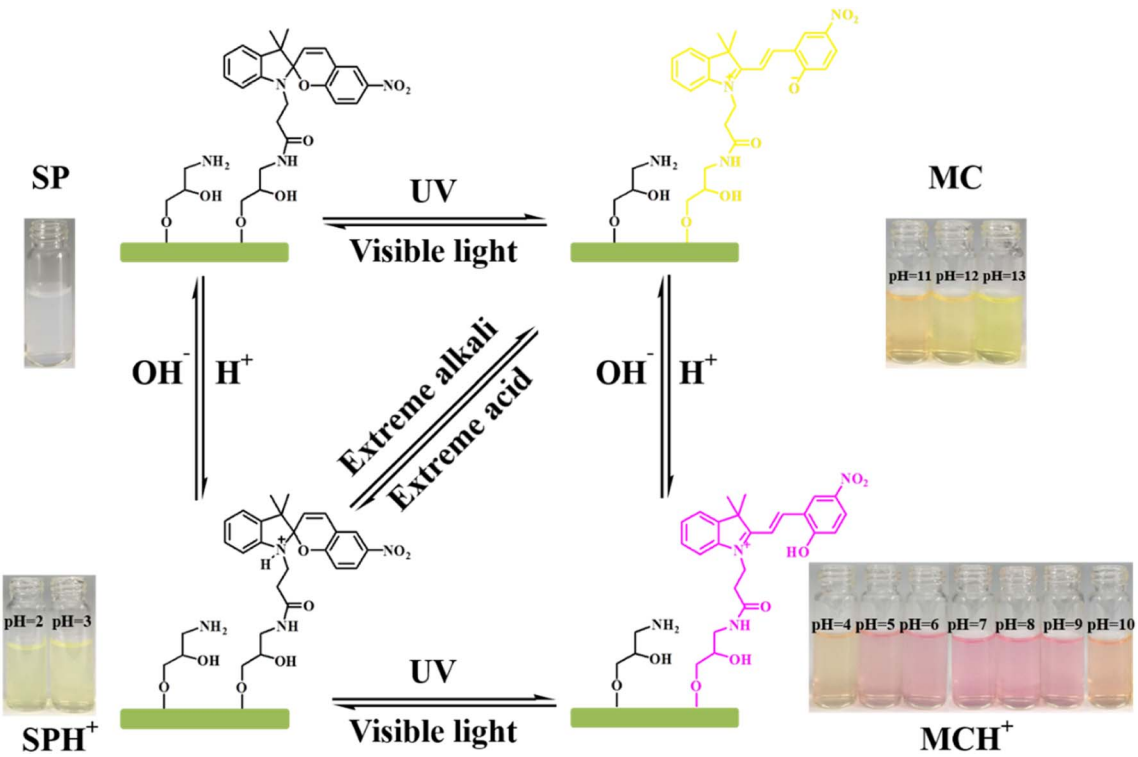

Fig. 8 Photochromism and acidochromism of spiropyran based on the reversible transformations between the four states: spiropyran (SP), merocyanine (MC), protonated spiropyran (SPH^+), and protonated merocyanine (MCH^+). Inset denotes the photographic images of SP-CNCs aqueous solution at different pH values (2, 3, 4, 5, 6, 7, 8, 9, 10, 11, 12 and 13).

Author contributions

X. Ye designed and performed the experiments, and drafted the manuscript; A. Wang and D. Zhang provided advices and performed the experiments; P. Zhou and P. Zhu advised the work; all the authors discussed the results and approved the manuscript.

Conflicts of interest

The authors declare no conflict of interest.

Acknowledgements

The authors would like to acknowledge the support from Shenzhen Science and Technology Innovation Commission (Grant No. JCYJ20190809111603608), Post-doctoral Foundation Project of Shenzhen Polytechnic (Grant No. 6021330019K0 and 6021330011K0), Innovation Project of Shenzhen Polytechnic (Grant No. CXGC2021C0003), Natural Science Foundation of Guangdong Province, China (Grant No. 2020A1515011194 and 2019B1515120013) and Guangdong Provincial General University Innovation Team Project (Grant No. 2020KCXTD047).

References

1 R. Suriano, R. Bernasconi, L. Magagnin and M. Levi, *J. Electrochem. Soc.*, 2019, **166**, B3274.
2 M. Bril, S. Fredrich and N. A. Kurniawan, *Smart Mater. Med.*, 2022, **3**, 257–273.
3 M. Mrinalini and S. Prasanthkumar, *ChemPlusChem*, 2019, **84**, 1103–1121.
4 B. Tian, Y. Liu and J. Liu, *Carbohydr. Polym.*, 2019, **24**, 3267.
5 F. Andrade, M. M. Roca-Melendres, E. F. Durán-Lara, D. Rafael and S. Schwartz, *Cancers*, 2021, **13**, 1164.
6 A. Grein-lankovski, A. Graillot, W. Loh and J. Berret, *Emergent Mater.*, 2021, **4**, 1351–1362.
7 V. Thakur, A. Guleria, S. Kumar, S. Sharma and K. Singh, *Mater. Adv.*, 2021, **2**, 1872–1895.
8 Y. Dai, X. Chen and X. Zhang, *Polym. Chem.*, 2019, **10**, 34–44.
9 A. A. Ali, R. Kharbash and Y. Kim, *Anal. Chim. Acta*, 2020, **1110**, 199–223.
10 K. Imato, K. Momota, N. Kaneda, I. Imae and Y. Ooyama, *Chem. Mater.*, 2022, **34**, 8289–8296.
11 A. A. Khuzin, A. R. Tuktarov, V. A. Barachevsky, T. M. Valova, A. R. Tulyabaev and U. M. Dzhemilev, *RSC Adv.*, 2020, **10**, 15888–15892.
12 M. Gan, T. Xiao, Z. Liu and Y. Wang, *RSC Adv.*, 2019, **9**, 12325–12330.
13 X. He, W. Xu, C. Xu, F. Ding, H. Chen and J. Shen, *Dyes Pigm.*, 2020, **180**, 108497.
14 B. Razavi, A. Abdollahi, H. Roghani-Mamaqani and M. Salami-Kalajahi, *Polymer*, 2020, **187**, 122046.
15 H. Xia, Y. Ding, J. Gong, A. Lilienkampf, K. Xie and M. Bradley, *ACS Appl. Mater. Interfaces*, 2022, **14**, 27107–27117.
16 F. Arjmand and Z. Mohamadnia, *Polym. Chem.*, 2022, **13**, 937–945.
17 L. Zheng, F. Seidi, Y. Liu, W. Wu and H. Xiao, *Eur. Polym. J.*, 2022, **177**, 111432.
18 Y. Cong, X. Wang, S. Zhu, L. Liu and L. Li, *ACS Appl. Bio Mater.*, 2021, **4**, 2790–2797.
19 B. Liao, P. Long, B. He, S. Yi, B. Ou, S. Shen and J. Chen, *J. Mater. Chem. C*, 2013, **1**, 3716–3721.
20 B. Liao, H. Lv, X. Deng, B. He and Q. Liu, *J. Nanopart. Res.*, 2017, **19**, 265.
21 A. K. Rana, E. Frollini and V. K. Thakur, *Int. J. Biol. Macromol.*, 2021, **182**, 1554–1581.
22 S. Xie, X. Zhang, M. P. Walcott and H. Lin, *Eng. Sci.*, 2018, **2**, 4–16.
23 J. Shojaeiarani, D. Bajwa and A. Shirzadifar, *Carbohydr. Polym.*, 2019, **216**, 247–259.
24 I. Lugoloobi, H. Maniriho, L. Jia, T. Namulinda, X. Shi and Y. Zhao, *J. Controlled Release*, 2021, **336**, 207–232.
25 Z. Zheng, C. Tang and J. T. W. Yeow, *Sens. Actuators, B*, 2020, **320**, 128596.
26 X. Sun, J. Li, Q. He, Y. Xue, Y. Bai, Y. Yang, X. Wang, S. Wang and R. Li, *RSC Adv.*, 2022, **12**, 16798–16804.
27 R. Li, Y. Liu, F. Seidi, C. Deng, F. Liang and H. Xiao, *Adv. Mater. Interfaces*, 2022, **9**, 2101293.
28 Y. He, H. Li, X. Fei and L. Peng, *Carbohydr. Polym.*, 2021, **252**, 117156.
29 R. Nasseri, C. P. Deutschman, L. Han, M. A. Pope and K. C. Tam, *Mater. Today Adv.*, 2020, **5**, 100055.
30 K. B. R. Teodoro, R. C. Sanfelice, F. L. Migliorini, A. Pavinatto, M. H. M. Facure and D. S. Correa, *ACS Sens.*, 2021, **6**(7), 2473–2496.
31 L. Chen, W. Wang, B. Su, Y. Wen, C. Li, Y. Zhou, M. Li, X. Shi, H. Du and Y. Song, *ACS Nano*, 2014, **8**, 744–751.
32 X. Ye, H. Wang, L. Yu and J. Zhou, *Nanomaterials*, 2019, **9**, 707.
33 Y. Qi, S. Lin, J. Lan, Y. Zhan, J. Guo and J. Shang, *Carbohydr. Polym.*, 2021, **260**, 117760.
34 O. Augusto, T. Dias, S. Konar, A. L. Leão and M. Sain, *Carbohydr. Polym.*, 2019, **220**, 79–85.
35 J. K. Rad, Z. Balzade and A. R. Mahdavian, *J. Photochem. Photobiol., C*, 2022, **51**, 100487.
36 M. S. A. Abdel-Mottaleb, M. Saif, M. S. Attia, M. M. Abo-Aly and S. N. Mobarez, *Photochem. Photobiol. Sci.*, 2018, **17**, 221–230.
37 A. Abdollahi, K. Sahandi-Zangabad and H. Roghani-Mamaqani, *ACS Appl. Mater. Interfaces*, 2018, **10**, 39279–39292.
38 Y. Yang, T. Zhang, J. Yan, L. Fu, H. Xiang, Y. Cui, J. Su and X. Liu, *Langmuir*, 2018, **34**, 15812–15819.
39 T. Zheng, Z. Xu, Y. Zhao, H. Li, R. Jian and C. Lu, *Sens. Actuators, B*, 2018, **225**, 3305–3315.
40 M. Schnurbu, M. Kabat, E. Jarek, M. Krzan, P. Warszynski and B. Braunschweig, *Langmuir*, 2020, **36**, 6871–6879.
41 A. Meeks, M. M. Lerch, T. B. H. Schroeder, A. Shastri and J. Aizenberg, *J. Am. Chem. Soc.*, 2022, **144**, 219–227.